View metadata, citation and similar papers at core.ac.uk
brought to you by CORE
provided by ScholarWorks@UNIST

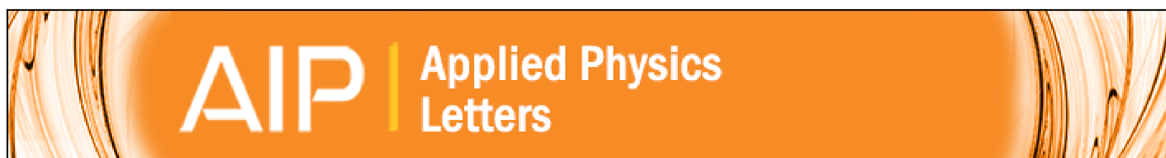


# Microscopic origin of bipolar resistive switching of nanoscale titanium oxide thin films

Hu Young Jeong, Jeong Yong Lee, Sung-Yool Choi, and Jeong Won Kim

Citation: Applied Physics Letters **95**, 162108 (2009); doi: 10.1063/1.3251784
View online: http://dx.doi.org/10.1063/1.3251784
View Table of Contents: http://scitation.aip.org/content/aip/journal/apl/95/16?ver=pdfcov
Published by the AIP Publishing

**Articles you may be interested in**
In-operando and non-destructive analysis of the resistive switching in the Ti/HfO2/TiN-based system by hard x-ray photoelectron spectroscopy
Appl. Phys. Lett. **101**, 143501 (2012); 10.1063/1.4756897

Effect of the top electrode materials on the resistive switching characteristics of TiO2 thin film
J. Appl. Phys. **109**, 124511 (2011); 10.1063/1.3596576

Effect of top electrode materials on bipolar resistive switching behavior of gallium oxide films
Appl. Phys. Lett. **97**, 193501 (2010); 10.1063/1.3501967

Hysteretic bipolar resistive switching characteristics in TiO 2 / TiO 2 − x multilayer homojunctions
Appl. Phys. Lett. **95**, 093507 (2009); 10.1063/1.3224179

Bipolar resistive switching in polycrystalline Ti O 2 films
Appl. Phys. Lett. **90**, 113501 (2007); 10.1063/1.2712777

This article is copyrighted as indicated in the article. Reuse of AIP content is subject to the terms at: http://scitation.aip.org/termsconditions. Downloaded to IP: 114.70.7.203 On: Wed, 19 Nov 2014 00:25:33

APPLIED PHYSICS LETTERS **95**, 162108 (2009)

# Microscopic origin of bipolar resistive switching of nanoscale titanium oxide thin films

Hu Young Jeong,[1] Jeong Yong Lee,[1,a)] Sung-Yool Choi,[2,b)] and Jeong Won Kim[3]
[1]*Department of Materials Science and Engineering, KAIST, Daejeon 305-701, Republic of Korea*
[2]*Electronics and Telecommunications Research Institute (ETRI), Daejeon 305-700, Republic of Korea*
[3]*Korea Research Institute of Standards and Science (KRISS), Daejeon 305-340, Republic of Korea*

(Received 10 April 2009; accepted 26 September 2009; published online 21 October 2009)

We report a direct observation of the microscopic origin of the bipolar resistive switching behavior in nanoscale titanium oxide films. Through a high-resolution transmission electron microscopy, an analytical transmission electron microscopy technique using energy-filtering transmission electron microscopy, and an *in situ* x-ray photoelectron spectroscopy, we demonstrated that the oxygen ions piled up at the top interface by an oxidation-reduction between the titanium oxide layer and the top Al metal electrode. We also found that the drift of oxygen ions during the on/off switching induced the bipolar resistive switching in the titanium oxide thin films. © *2009 American Institute of Physics*. [doi:10.1063/1.3251784]

The bistable switching phenomenon, reversible switching between a high resistance state and a low resistance state, has been discovered for various binary oxide films such as NiO,[1] $Nb_2O_5$,[2] $Al_2O_3$,[3] $SiO_2$,[4] and $TiO_2$.[5] Since the recent publication by Baek *et al.*[6] in 2004, resistive random access memory (RRAM) using simple binary transition metal oxides such as NiO and $TiO_2$ has attracted extensive attention as a high-potential next-generation nonvolatile memory (NVM) due to its simple process, simple device structure, and high complementary metal-oxide-semiconductor compatibility.[7–9] In the fundamental point of view, the electrical properties of nanoscale binary oxide thin films give the deeper understanding of the recently rediscovered memristor, the missing component of the basic circuits elements. Hewlett–Packard (HP) group[10–12] suggested that the motion of dopants or impurities, such as oxygen vacancies acting as mobile +2 charged dopants, was able to produce remarkable changes in the device resistance (memristic behavior), especially in $TiO_{2-x}$ devices. To verify the above model, it is crucial to identify the origin and movement of oxygen vacancies in the actual devices. However, researchers have not yet fully shown a direct evidence of the movement of oxygen vacancies.

In this letter, we report on the presence and movement of oxygen vacancies formed by a redox reaction at the $Al/TiO_2$ top interface through a high-resolution transmission electron microscopy (HRTEM), an analytical TEM technique using energy-filtering transmission electron microscopy (EFTEM), and an *in situ* x-ray photoelectron spectroscopy (XPS).

To fabricate the $Al/TiO_2/Al$ memory device, the $TiO_2$ oxide film with a thickness of ~16 nm was deposited on an $Al/SiO_2/Si$ substrate by the plasma enhanced atomic layer deposition (PEALD) (ASM Genitech MP-1000) 400 cycle process at a substrate temperature of 180 °C. Titanium (IV) tetra-iso-propoxide (TTIP) precursor was used with oxygen plasma as the oxidizing agent. One cycle of $TiO_2$ growth consisted of the sequential injection of TTIP (2 s), Ar (4 s), $O_2$ gas [150 SCCM (SCCM denotes standard cubic centimeter per minute), 2 s], and Ar (2 s). rf plasma was only activated during the injection of $O_2$ gas for 1.5 s with rf power of 150 W. The 50-nm-thick aluminum bottom and top electrode were deposited by thermal evaporation method, forming the cross-bar type structures using a shadow mask with a line width of 60 $\mu$m. The cross-sectional images and chemical analyses of $Al/TiO_2/Al$ samples were examined by HRTEM and analytical TEM. A 300 kV JEOL JEM 3010 with a 0.17 nm point resolution and a high-voltage electron microscope JEOL ARM-1300 operating at 1250 keV equipped with energy-filtering TEM were used. The XPS spectra were measured using Mg $K\alpha$ radiation ($\hbar\omega$ =1253.6 eV) and a SES100 analyzer (Gamadata) equipped with a two-dimensional charge-coupled device detector, both of which give a total energy resolution of 0.9 eV for each core level measurement. Using a thermal evaporation cell, the Al was deposited on $TiO_2$ film in a high vacuum chamber with a deposition rate of 0.25 nm $min^{-1}$. After the Al deposition, the sample was transferred to an analysis chamber without exposure to air for the XPS measurement. The electrical property (*I-V* curve) was measured using a Keithley 4200 Semiconductor Characterization System in a dc voltage sweep mode.

Figure 1 shows the typical *J-V* characteristic of an $Al/TiO_2/Al$ memory cell measured at room temperature un-

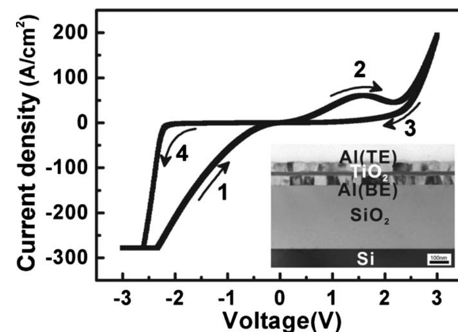


FIG. 1. Current density-voltage (*J-V*) characteristics of a typical $Al/TiO_2/Al$ memory device. Cross-sectional BFTEM image of $Al/TiO_2/Al$ sandwiched structure deposited on a $SiO_2$ (3000 Å)/Si substrate is shown in the right bottom inset.

a)Electronic mail: j.y.lee@kaist.ac.kr.
b)Electronic mail: sychoi@etri.re.kr.



This article is copyrighted as indicated in the article. Reuse of AIP content is subject to the terms at: http://scitation.aip.org/termsconditions. Downloaded to IP: 114.70.7.203 On: Wed, 19 Nov 2014 00:25:33

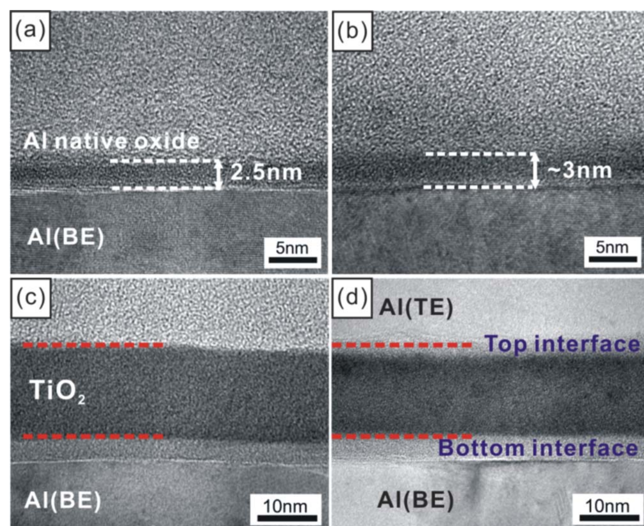


FIG. 2. (Color online) A series of the cross-sectional HRTEM images of $Al/TiO_2/Al$ structures observed step by step: (a) Image showing the existence of native aluminum oxide at the aluminum metal surface. (b) Image indicating the broadening of native aluminum oxide by the thermal annealing. (c) Image obtained after depositing amorphous titanium oxide thin film by a 400 cycle PEALD process. (d) Completed cell image after thermal evaporation deposition of the aluminum top electrode.

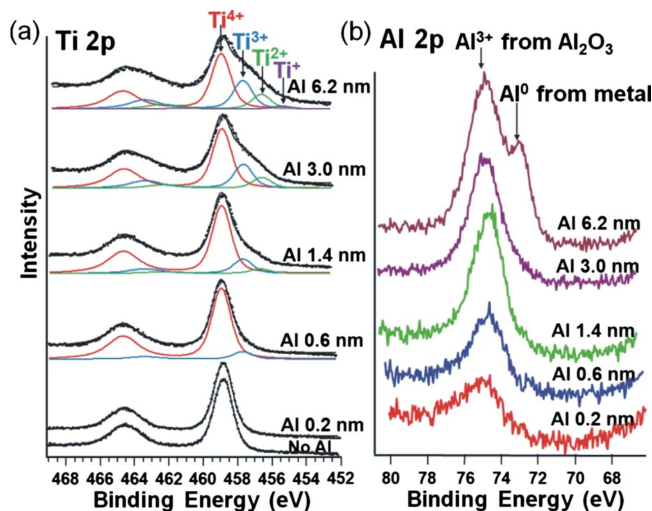


FIG. 3. (Color online) XPS spectra of (a) Ti 2*p* and (b) Al 2*p* measured as a function of Al thickness on amorphous titanium oxide film deposited by the PEALD process.

der the dc voltage sweep. The *J-V* curve exhibits a clear hysteretic and asymmetric behavior. Bistable resistance switching between a high-resistance state and a low-resistance state was induced by the opposite polarity of the applied voltage. The negative voltage (−3 V) changed the pristine device to the on state, indicating no "forming" procedure which is a prerequisite for the $Pt/TiO_2/Pt$ devices.[10–12] It was reported by Yu *et al.*[13] that this bipolar resistive switching was associated with the charge trap sites in the top domain of the Ti oxide thin layer. The right bottom inset of Fig. 1 shows a cross-sectional bright-field (BF) TEM image of the $Al/TiO_2/Al$ structure with three distinctive layers (the Al bottom electrode, the Ti oxide thin layer, and the Al top electrode). It reveals that the highly uniform Ti oxide layer has been deposited due to the excellent roughness of an Al bottom electrode and the self-limited surface reaction of the ALD method.

To clearly characterize the interface regions, we performed the HRTEM measurements of the sequential samples during the fabrication processes. Figure 2 is a series of cross-sectional HRTEM images of stacked $Al/TiO_2/Al$ layers which were observed sequentially before and after depositing the titanium oxide thin layer. Note that the very thin native aluminum oxide with a 2–3 nm thickness had already been present before the ALD process, as shown in Fig. 2(a). Figure 2(b) displays the HRTEM image of the surface of the Al bottom electrode annealed at 180 °C, that is, the same temperature as the ALD process chamber. It can be inferred that the native aluminum oxide expands to the ~3 nm thickness due to a thermal annealing effect during the specimen loading process in the ALD main chamber. In Fig. 2(c), it can be seen that the as-deposited titanium oxide layer with a dark contrast clearly has an amorphous phase with a thickness of ~16 nm. After the aluminum thermal evaporation process, the top interface layer was formed on the titanium oxide thin film, showing the amorphous phase with a light contrast, as shown in Fig. 2(d). In addition, it is remarkable that the top domain of the titanium oxide layer also has a light contrast, as compared with Fig. 2(c). [See the red dotted lines in Figs. 2(c) and 2(d).] It is believed that the composition of the upper Ti oxide layer has been drastically changed due to the reaction with the top aluminum metal layer during the deposition process. Generally, aluminum is well known as one of the most readily oxidizable metals. Therefore, aluminum atoms easily attract oxygen atoms from the titanium oxide layer and react with them, forming an interfacial Al oxide layer.[14] This oxidation-reduction process induces the oxygen vacancies in the region of titanium oxide.

To confirm the chemical reaction between the amorphous titanium oxide and the aluminum top electrode, XPS was also estimated. Dake and Lad[15] reported that aluminum strongly reduced the single crystal $TiO_2$ surface and an aluminum oxide was formed at the interface using x-ray and ultraviolet photoelectron spectroscopies. However, it has yet not been confirmed whether a similar reaction could occur at metal-amorphous $TiO_2$ interfaces. For this experiment, an *in situ* XPS measurement was carried out upon growing ultrathin aluminum metal layers on the amorphous titanium oxide. Figure 3 shows the XPS spectra of Ti 2*p* and Al 2*p* measured as a function of aluminum deposition thickness. For the amorphous titanium surface, Ti cations are all in the $Ti^{4+}$ state at a binding energy of 458.9 eV, as shown in the lowest curve of Fig. 3(a). By increasing the aluminum dose, a shoulder at the low binding energy side of Ti 2*p* spectra emerges and these spectra can be deconvoluted to show the contributions by a series of different oxidation states ($Ti^{3+}$, $Ti^{2+}$, and $Ti^{+}$), as indicated in Fig. 3(a). This clearly confirms that amorphous titanium oxide surface is reduced and the amount of reduced titanium oxide increases with additional aluminum doses. On the contrary, Fig. 3(b) represents that the Al 2*p* spectra first appears in the $Al^{3+}$ state, which corresponds to the oxidized state of Al. The $Al^{3+}$ intensity increases until the aluminum thickness reaches 3 nm. However, an Al metallic state ($Al^0$) appears at the thickness of 6.2 nm. This shows that aluminum oxide phases with a thickness of 3–6 nm are usually formed before metallic aluminum phases become stable, which is clearly consistent with the HRTEM images. The XPS results suggest that the aluminum

This article is copyrighted as indicated in the article. Reuse of AIP content is subject to the terms at: http://scitation.aip.org/termsconditions. Downloaded to IP: 114.70.7.203 On: Wed, 19 Nov 2014 00:25:33

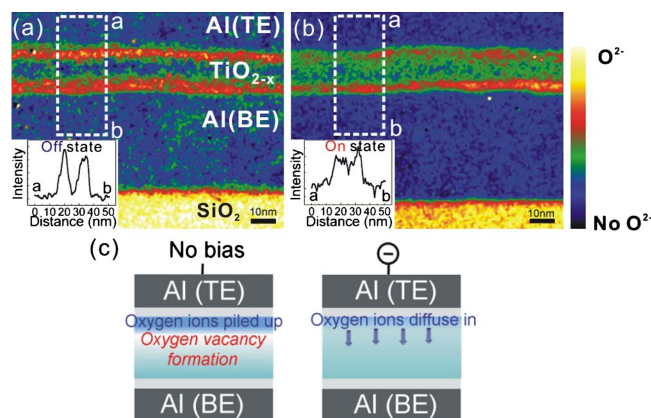


FIG. 4. (Color online) Energy filtered-TEM elemental (oxygen) maps of two different samples (the off and on state): (a) EELS based oxygen elemental map of as-grown $Al/TiO_2/Al$ structure, corresponding to the off state. (b) Oxygen elemental map of the sample applied negative set bias (−3 V) on the top Al electrode, corresponding to the on state. The left insets are the corresponding average intensity profiles obtained from the white rectangular areas. (c) Schematics of the proposed model for bipolar resistive switching of $Al/TiO_2/Al$ device.

is readily oxidized by extracting oxygen ions from the amorphous titanium oxide surface, causing titanium reduced.

The chemical change of an amorphous titanium oxide thin layer sandwiched between two aluminum electrodes, in the real off and on states, was characterized using electron energy loss spectroscopy (EELS) analysis. EELS elemental mapping was obtained using the "three window technique."[16] Figures 4(a) and 4(b) show EELS energy-filtered oxygen maps of each memory state and corresponding intensity profiles of the regions marked with white rectangular areas, visualizing the distribution of oxygen. One remarkable finding is the oxygen deficiency existing in the middle region of titanium oxides. Many researchers have believed that oxygen vacancies at the metal-oxide interface performed the critical function of bistable resistive switching. However, from the above the EELS results, it is found that the oxygen concentration at the interface very close to aluminum top electrode is much higher than that of the inner part, as displayed with red color. This can be explained via an oxygen diffusion process. When the interaction between aluminum and titanium oxide occurred at the top interface, the insufficient oxygen ions was added continuously from the below bulk domain. As a result, the bulk region underneath the top interface became more oxygen deficient than the top interface. Furthermore, the EELS oxygen mapping image of the on state, displayed in Fig. 4(b), remarkably shows that oxygen ions driven at the top interface region rediffused into the inner titanium oxide part. It is strongly confirmed that oxygen ions are able to move in the $TiO_{2-x}$ amorphous active layer by a strong external electric field, as reported by other groups.[12,17]

Based on above results, the bipolar switching mechanisms of our $Al/TiO_2/Al$ devices can be described schematically in Fig. 4(c). When the top Al electrode deposition started in the thermal evaporation chamber and aluminum atoms attached to the surface of the titanium oxide, they gathered oxygen ions present on the top $TiO_2$ layer, resulting in the formation of the top interface amorphous layer owing to strong oxygen affinity of Al metal. The top interface may be Al–Ti–O phases. Therefore, the oxygen deficient domain was created at the bulk $TiO_2$ region. This state corresponds to the off state in $Al/TiO_2/Al$ memory devices. When a sufficient negative bias is applied to the top Al electrode, the negatively charged oxygen ions piled up at the vicinity of Al–Ti–O layer diffuse into the inner bulk $TiO_{2-x}$ region, causing the device to switch to the on state.

In summary, we have demonstrated that the drift of oxygen ions (vacancies) by the applied bias was attributed to the microscopic origin of the bistable resistivity switching of $Al/TiO_2/Al$ devices. From the sequential cross-sectional HRTEM images, *in situ* XPS measurement, and EFTEM elemental mapping analysis, it is justified that oxygen ions piled up at top interface region can drift as external bias exceeds the threshold field. These analyses give the direct evidence of the memristic behaviors and the deeper understanding of the bipolar resistive switching mechanisms of binary oxides.

This work was supported by the Next-generation Nonvolatile Memory Program of the Ministry of Knowledge Economy (10029953-2009-31) and the Korea Research Foundation Grant (MOEHRD) (KRF-2008-005-J00902). The authors sincerely thank Youn-Joong Kim at Korea Basic Science Institute (KBSI) for the use of the high-voltage electron microscope and the technical staff of the Process Development Team at ETRI for their support with the PEALD facility.

[1]J. F. Gibbons and W. E. Beadle Solid-State Electron. **7**, 785 (1964).
[2]W. R. Hiatt and T. W. Hickmott, Appl. Phys. Lett. **6**, 106 (1965).
[3]F. Argall, Electron. Lett. **2**, 282 (1966).
[4]R. W. Brander, D. R. Lamb, and P. C. Rundle, Br. J. Appl. Phys. **18**, 23 (1967).
[5]F. Argall, Solid-State Electron. **11**, 535 (1968).
[6]I. G. Baek, M. S. Lee, S. Seo, M. J. Lee, D. H. Seo, D.-S. Suh, J. C. Park, S. O. Park, H. S. Kim, I. K. Yoo, U.-I. Chung, and J. T. Moon, Tech. Dig. - Int. Electron Devices Meet. **2004**, 587.
[7]I. G. Baek, D. C. Kim, M. J. Lee, H.-J. Kim, E. K. Yim, M. S. Lee, J. E. Lee, S. E. Ahn, S. Seo, J. H. Lee, J. C. Park, Y. K. Cha, S. O. Park, H. S. Kim, I. K. Yoo, U.-I. Chung, J. T. Moon, and B. I. Ryu, Tech. Dig. - Int. Electron Devices Meet. **2005**, 750.
[8]M.-J. Lee, S. Seo, D.-C. Kim, S.-E. Ahn, D. H. Seo, I.-K. Yoo, I. G. Baek, D.-S. Kim, I.-S. Byun, S.-H. Kim, I.-R. Hwang, J.-S. Kim, S.-H. Jeon, and B. H. Park, Adv. Mater. **19**, 73 (2007).
[9]M.-J. Lee, Y. Park, D.-S. Suh, E.-H. Lee, S. Seo, D.-C. Kim, R. Jung, B.-S. Kang, S.-E. Ahn, C. B. Lee, D. H. Seo, Y.-K. Cha, I.-K. Yoo, J.-S. Kim, and B. H. Park, Adv. Mater. **19**, 3919 (2007).
[10]J. J. Yang, M. D. Pickett, X. Li, D. A. A. Ohlberg, D. R. Stewart, and R. S. Williams, Nat. Nanotechnol. **3**, 429 (2008).
[11]D. B. Strukov, G. S. Snider, D. R. Stewart, and R. S. Williams, Nature (London) **453**, 80 (2008).
[12]J. J. Yang, F. Miao, M. D. Pickett, D. A. A. Ohlberg, D. R. Stewart, C. N. Lau, and R. S. Williams, Nanotechnology **20**, 215201 (2009).
[13]L.-E. Yu, S. Kim, M.-K. Ryu, S.-Y. Choi, and Y.-K. Choi, IEEE Electron Device Lett. **29**, 331 (2008).
[14]U. Diebold, Surf. Sci. Rep. **48**, 53 (2003).
[15]L. S. Dake and R. J. Lad, Surf. Sci. **289**, 297 (1993).
[16]L. Reimer, *Energy-Filtering Transmission Electron Microscopy* (Springer, Berlin, 1995), p. 387.
[17]W. Shen, R. Dittmann, U. Breuer, and R. Waser, Appl. Phys. Lett. **93**, 222102 (2008).

This article is copyrighted as indicated in the article. Reuse of AIP content is subject to the terms at: http://scitation.aip.org/termsconditions. Downloaded to IP: 114.70.7.203 On: Wed, 19 Nov 2014 00:25:33